JAAS

View Online
Dynamic Article Links

Cite this: DOI: 10.1039/c1ja10242g

www.rsc.org/jaas

COMMUNICATION

Direct chemical analysis of frozen ice cores by UV-laser ablation ICPMS

Wolfgang Müller,*[a] J. Michael G. Shelley[b] and Sune Olander Rasmussen[c]

Received 12th August 2011, Accepted 26th September 2011
DOI: 10.1039/c1ja10242g

Cryo-cell *UV*-LA-ICPMS is a new technique for direct chemical analysis of frozen ice cores at high spatial resolution (<300 μm). It was tested in a pilot study on NGRIP ice and reveals sea ice/dust records and annual layer signatures at unprecedented spatial/time resolution. Uniquely, the location of cation impurities relative to grain boundaries in recrystallized ice can be assessed.

Introduction

Polar ice cores are continuous, high-resolution archives of past climate variability on Earth.[1,2] Whereas Greenland ice cores provide an unprecedented record of climate variation of the last glacial period up to ~125,000 years,[3] the lower ice accumulation in Antarctica means that older ice (~800,000 years) with several glacial-interglacial cycles is preserved.[4]

Accurate dating of ice cores is paramount for a comparison with other climate archives, which ultimately allows an assessment of climate leads and lags and opens up an understanding of climate dynamics. Whenever possible, dating of ice cores is achieved by layer counting, which for the Greenland cores furnished a new time scale (GICC05) *via* multi-proxy based counting.[5] These include physical (optical) and chemical properties such as seasonally varying cation (*e.g.* Ca, Na) and anion (*e.g.* NO_3, SO_4) concentrations measured by continuous flow analysis (CFA) of melted ice with an effective resolution of >10 mm.[5,6] Recently, sub-annual resolution analysis of melted Greenland ice cores have established the relative timing and dynamics of rapid climate change (*e.g.* the so-called 'DO-events'). These show that temperatures of the Greenland moisture source switched within 1–3 years[7] and reveal the relative sequence between wind (dust), precipitation and temperature at 2 mm spatial resolution.[8] Hence, extracting data from ice cores at highest temporal/spatial resolution is crucial in order to unravel mechanisms underlying such rapid climate events,[9] as well as for identifying sub-cm thin annual layers. Furthermore, direct *in situ* chemical analysis of frozen ice can reveal the locations of cation impurities relative to grain boundaries, and whether these become modified during recrystallization of ice with increasing depth.

[a]*Department of Earth Sciences, Royal Holloway University of London, Egham, Surrey, TW20 0EX, UK. E-mail: w.muller@es.rhul.ac.uk*
[b]*Laurin Technic P/L, Canberra, ACT, 2604, Australia*
[c]*Centre for Ice and Climate, Niels Bohr Institute, University of Copenhagen, Denmark*

Using 193 nm excimer laser-ablation ICPMS (UV-LA-ICPMS), we present a new methodology for direct *in situ* chemical analysis of *frozen* ice cores (Fig. 1). Because this methodology avoids melting, all spatial relationships within frozen ice can be directly assessed and chemical analysis at <300 μm scale is possible. Ice is essentially

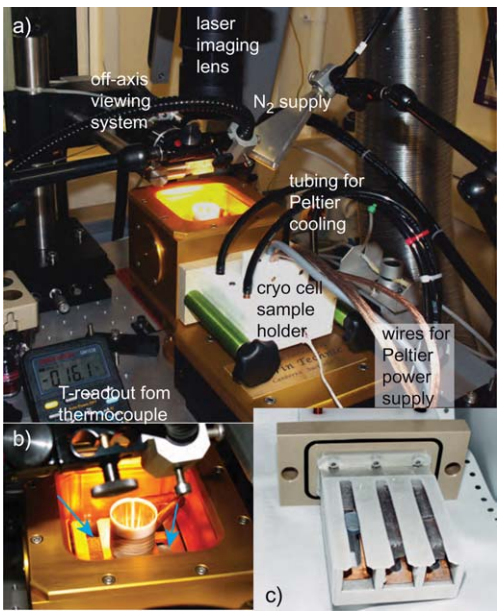

Fig. 1 (a) Cryo-cell UV-LA-ICPMS setup used in this study. A custom-built cryo-sample holder is loaded into a standard Laurin two-volume laser-ablation cell (Ref. 13). The sample holder made of anodized aluminium is capable of holding three strips of 50 mm long ice (b, c); its 'tongue-like' extension through the cell door has a Peltier element clamped to each side to cool the entire aluminium-holder. A heat sink in form of a Cu-block is connected to the hot side of each Peltier element, which in turn is cooled by cooling water (4 lines of black tubing). The two Peltier elements are fed by low voltage-high current electrical cables. An electronic proportional controller controls temperature and detects whether the cooling water is flowing. Frosting of the laser cell window is prevented by a continuous bleed of N_2 across its top. The temperature inside the sample holder is monitored using a digital multi-meter connected to a thermocouple, and ranges between −25 °C without He flow and −16 °C with He flowing through cell; this rise is because He currently is not pre-cooled. (b) Inside view of the cryo-holder with an ice strip and a NIST612 disc visible (arrow left and right of funnel). (c) Cryo-holder with two ice strips and a NIST612 disc mounted, which are lifted against the laser focus plane by teflon-coated Cu-Be-springs.

opaque at 175 nm and shows an enormous increase in absorption between 200 and 175 nm over some 10 orders of magnitude.[10] This contribution investigates ice ablation at 193 nm, the now commonly used excimer wavelength. The only prior attempt at analyzing glacial ice by LA-ICPMS[11] utilized a very different analytical setup, namely an IR laser (1064 nm) as well as a LA cell cooled by a cryogenic liquid and much larger volume.[12]

Materials and methods

A custom-built (Laurin Technic, Australia), peltier-cooled cryogenic sample holder, uniquely compatible with the two-volume Laurin LA cell, is used with the RESOlution M-50 excimer (193 nm) LA system prototype,[13] and in turn coupled to an Agilent 7500cs ICPMS operated in collision/reaction-cell mode. Up to three 50 mm strips of ice core ice (~12 mm thick and ~13 mm wide) can be mounted together in the cryo-sample holder constructed from anodized aluminium. Samples are kept below minus 20 °C using water-cooled Peltier elements; when using a flow of non-precooled He carrier gas, the cell temperature rises to slightly above −20 °C (Fig. 1). Ice strips are held in position and lifted against the reference surface by teflon-coated Cu-Be springs. The aperture-imaging beam delivery system allows both large rectangular (>500 μm long axis) or up to 300 μm circular spots to be used; large spot sizes are necessary in view of the low (ppb) concentrations of normal major cations in Greenland ice. UV-LA at 193 nm couples well to glacial ice despite the strongly decreasing absorption between 175 and 200 nm[10] (Fig. 2). Using fluences of ~2–4 J cm^{-2}, highly controlled ablation of ice takes places as shown in the sequence of developing craters in Fig. 2. Grain boundaries also do not appear to inhibit ice ablation at 193 nm, neither for tracks nor spots (Fig. 2a). The smooth crater morphology demonstrates controlled ablation of ice, which contrasts with the rugged crater morphology obtained by IR-LA[12] (using significantly higher laser energy). Based on optically estimated crater depths of 80–100 μm for 800 laser pulses (Fig. 2), we estimate 0.1–0.15 μm ice removal per pulse, which is a factor of approximately 5000 less than the ~30 μg of ice removed per laser pulse using the IR system.[12] Frosting of the LA cell window due to condensation of humid ambient air that would lead to significant changes in laser fluence is prevented by directing a flow of high-purity nitrogen across the LA cell (Fig. 1). The signal uniformity and rapid washout of the Laurin LA cell[13] allows acquisition of compositional data using both continuous lateral profiling and depth-profiling of ice (Fig. 3).

The ice samples used in this pilot study are from the Greenland NGRIP ice core[3] and are ~19.2 ka b2k old (b2k: before A.D. 2000). A few 50 mm long, 13 mm wide and 12 mm thick ice strips were cut from close to the outer portion of the drill core; each 50 mm sample represents approximately two years. Only limited initial mechanical cleaning was conducted after cutting. Chemical analysis of cations, present in both soluble and particulate form, by LA-ICPMS focused on the analysis of major elements (Mg, Al, Ca, Fe, Mn) in sub-ppm-concentrations in Greenland ice (particles are not resolvable in ice using the viewing optics of the LA system). There, a typical seasonal cycle for warmer periods includes a sea salt peak (Na, Mg) in late winter, followed by a dust peak (Ca, Al, Fe) in spring and enhanced [SO_4^{2-}], [NO_3^-] and [NH_4^+] during summer,[5,6] but in colder intervals all impurity peaks may coincide. Laser-ablation of ice took place in He to which Ar and 7–8 ml min^{-1} H_2, the latter as additional diatomic gas to enhance sensitivity of low mass elements,[14] was added downstream of the LA cell (see Table 1 for analytical details). H_2 is preferred over N_2 because the latter has adverse influence on backgrounds for *e.g.* mass 27 (^{27}Al). The Agilent 7500 ICPMS was fitted

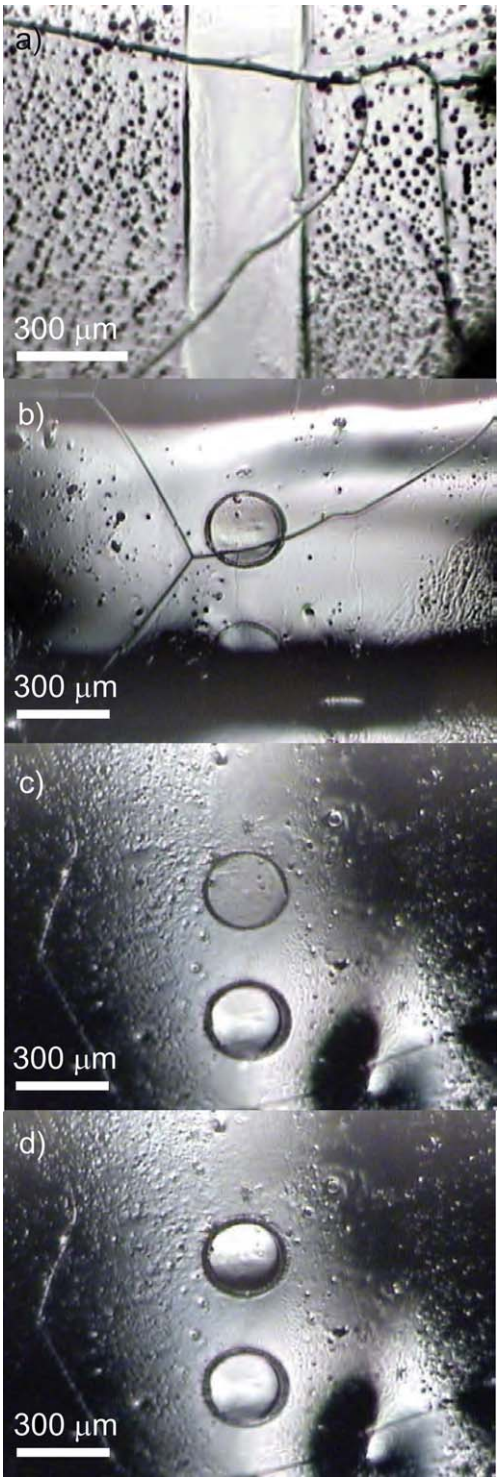

Fig. 2 Optical images (taken with camera of the laser-ablation system) of both laser-ablated tracks (a) and circular craters (b–d) in natural ice from Greenland (NGRIP). Grain boundaries (a, b) are no obstacle to controlled ablation of ice; a developing crater (top) is shown in the c&d-sequence. Overall, these images illustrate the very controlled ablation of glacial ice using a 193 nm excimer laser (~4 J cm^{-2}).

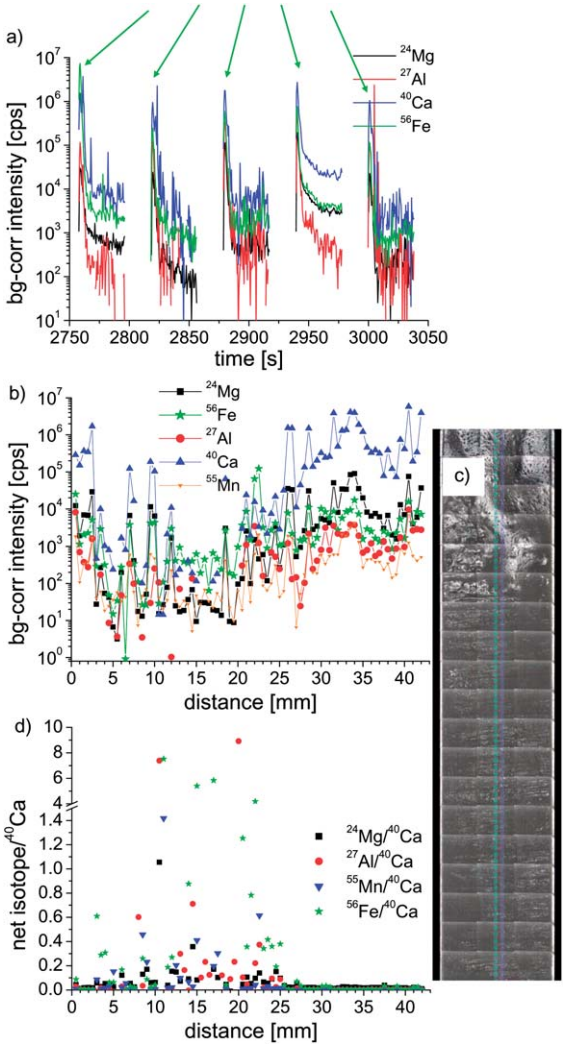

Fig. 3 (a) Background-corrected intensities for Mg, Al, Ca, Fe of five consecutive laser spots (280 μm, 40 s, 20 Hz, 500 μm spacing) in NGRIP ice (~19.2 ka b2k), plus 20 s background before and after. The large signal decreases (green arrows) for the first few seconds are interpreted to reflect surface contamination, but the remainder represents compositionally heterogeneous ice. (b) Summary of net signals of a 43 mm long section of the NGRIP ice core (500 μm spot spacing, image shown in (c)) where averages of the last 20 s of signal for each spot are shown for 5 isotopes plotted relative to distance (mm). There is remarkable small-scale variability, which is exemplified in (d), where net isotopes are ratioed to the largest analyte signal ^{40}Ca. See text for details.

with the cs-lens that enables better low-mass enhanced tuning and was operated in collision/reaction-cell mode with H_2 gas. Charge transfer reactions of H_2 with ^{40}Ar and ^{40}Ar^{16}O inside the collision cell facilitate the complete removal of these intense plasma based interferences and open up access to the major Ca and Fe isotopes, ^{40}Ca and ^{56}Fe, necessary to achieve low-ppb LODs.[15] Addition of 3–3.5 ml min^{-1} H_2 (99.9999%) and careful KED lens settings thus achieves typical LODs for Mg, Al, Ca, Fe of 1.3, 31, 32, and 12 ppb, respectively (280 μm spots, 20 Hz). Under these conditions, presence of hydrides and oxides were carefully monitored on NIST612 (with ice strips being present in the LA cell) *via* ^{232}Th, ^{238}U and ^{209}Bi and their respective uninterfered hydride and oxide masses at 233, 239, 210 and 248, 254, 225 respectively, and found to be below 0.1%, with ThO/Th at 0.2%.

Results

Initial analyses were conducted as lateral profiles using a rectangular spot size of 500 × 50 μm to assess the extent of necessary pre-cleaning. Data were acquired of three rapid pre-cleaning passes at high repetition rates and scan speed (30 Hz, 10 mm min^{-1}), followed by one slower profile (30 Hz, 5 mm min^{-1}). The resultant irregular composition showed that laser-based pre-cleaning may not have been extensive enough everywhere. As a result, any further data acquisition thus involved drilling of 280 μm diameter spots at 20 Hz for 40 s (800 pulses; plus 20 s background), regularly spaced at 500 μm ('spots along a path'). Results of five representative, consecutive spots show rapidly decreasing background-corrected net-signals for ^{24}Mg, ^{27}Al, ^{40}Ca and ^{56}Fe (up to 3 orders of magnitude) for the first approximately 5–10 s, followed by a gentle decrease more typical of spot drilling for the remainder of the analysis, but some spots also show more internal variability, even increases (Fig. 3a). The rapid initial decrease (<10 s) is interpreted to reflect surface contamination, whereas the remainder of the individual analyses reflects compositionally variable ice. Up to an order of magnitude compositional variability is evident on a ~1 mm scale. Compositional data of ^{24}Mg, ^{27}Al, ^{40}Ca, ^{55}Mn and ^{56}Fe of a full 43 mm NGRIP ice strip analyzed at 500 μm resolution are presented in Fig. 3b–d, with the associated image of all 83 spots (280 μm diameter) in Fig. 3c. These plots show the signal averages of all isotopes during the last 20 s of each spot relative to distance along the ice strip and reveal a remarkable small-scale compositional variability. All isotopes show decreasing signals for the first ~12 mm interrupted by some large but very short peaks (~1 mm), followed by low signals up to ~21 mm and a further increase after from ~23 mm onwards. The overall variation is nearly 4 orders of magnitude for Ca and Fe, with slightly less variation characterizing Mg, Al and Mn. While Ca is the strongest analyte signal for the most part, for the interval between ~12–23 mm this is reversed with Fe becoming the highest signal and Al being below LOD for some of this interval. The contrasting relative analyte intensities are even more apparent when net isotope signals are ratioed against the largest signal (^{40}Ca, Fig. 3d). Between ~12–24 mm all analyte ratios increase substantially from values below 0.5 up to 10 (note the break in the ordinate scale), confirming that compositionally different source(s) are represented in this part of ice relative to the immediately adjacent high Ca ice. Preliminary results of similar yet lower resolution analyses over several strips of ice core confirms the existence of distinct (sub-) mm compositional variation in NGRIP ice.

Discussion

The net analyte signals (Fig. 3) have not yet been converted into concentrations. Two possibilities exist, namely using external standardisation *via* homogenous ice standards of known concentration, or a combination of internal/external standards, *e.g.* using OH (m/z = 17) as internal standard. The production of homogenous ice is difficult but possible using nebulization onto frozen surfaces or shock-freezing of very small volumes;[16] preliminary results of shock-frozen ~5 cm^3 dilute ICP standard solutions though showed significant inhomogeneity as evidenced during LA drilling. Even without

Table 1 Operating conditions of cryo-cell UV laser-ablation ICPMS (see text for further details)

ICPMS: Agilent 7500*cs*	
RF power	1300–1350 W
Sampling depth	5.5 mm
Carrier gas flow (Ar)	approx. 550–650 ml min^{-1} (optimized daily)
Coolant gas flow	15 l min^{-1}
Auxilliary gas flow	1 l min^{-1}
Dwell time/mass and Sweep duration	65 ms: ^{24}Mg, ^{27}Al, ^{40}Ca, ^{55}Mn, ^{56}Fe; 50 ms: ^{44}Ca; 20 ms: ^{65}Cu, ^{88}Sr, ^{140}Ce, ^{208}Pb; 490 ms
Collision/reaction cell gas	H_2 (99.9999 %), 3.5 ml min^{-1}
Monitored masses (*m*/*z*)	^{24}Mg, ^{27}Al, ^{40}Ca, ^{44}Ca, ^{55}Mn, ^{56}Fe, ^{65}Cu, ^{88}Sr, ^{140}Ce, ^{208}Pb
Sampler, skimmer cones	Ni
Extraction lenses	cs (tuning optimized for low masses)
OctP Bias	−23
QP Bias	−18
QP Focus	−8
$^{232}Th/^{238}U$	>0.90
ThO/Th (248/232)	<0.5%, typically 0.2%
Laser-ablation system RESOlution M-50 (prototype)	
Laser and wavelength	193 nm excimer (CompexPro 110)
Energy density (fluence) on target	2–4 J cm^{-2}
He gas flow	800–850 ml min^{-1}
H_2 carrier gas flow addition	5–8.5 ml min^{-1}
Laser repetition rate	20 Hz
Laser spot size (circular)	280 μm
Laser spot size (rectangular)	500 × 50 μm
Laser acquisition mode	Chain of spots, 500 μm spacing
Ar, H_2 carrier gas	Admixed downstream of LA cell
Signal smoothing	'Squid' included (but not really necessary at 20 Hz)
Cryo cell sample holder	
Cooling mechanism	Two Peltier elements
Sample holder temperature	−25°C (without He), −16°C (with He)
Holder material	Anodized aluminium

conversion into concentrations, our background-corrected analyte ratios are an effective way of highlighting unprecedented compositional variability at the <0.5 mm scale (Fig. 3c). The ~12 mm section of elevated isotope/^{40}Ca ratios appears to be compatible with approximately half a year, hence seasonal duration, given the ~22 mm of ice/year at 19.2 ka in NGRIP. Such net ratios are similar *e.g.* to data from XRF core scanners.[17]

In comparison to the only other LA-ICPMS work on ice cores by IR-LA-ICPMS,[11,12] the performance and analytical figures of merit of UV-LA-ICPMS of ice presented here are very different. Using a low fluence of 2–4 J cm^{-2}, UV-LA at 193 nm does allow very controlled, arguably more controlled than IR-LA, removal of ice by laser-ablation despite the nominally lower absorption coefficient of ice at 193 relative to 1064 nm. We interpret this to be due to the extremely large absorption coefficient increase at ~200 nm,[10] because also liquid water—if it was formed as thin films during early stages of UV-LA—has a similarly low absorption at ~200 nm and would not significantly influence the overall absorption characteristics. It follows that the other common UV-wavelengths used for laser-ablation, namely 213 and 266 nm, will not be suitable for ice-ablation, because they are offset to even lower absorption when compared to that of the ArF excimer wavelength at 193 nm. Our removal of ice per pulse estimated from crater depth and spot sizes (Fig. 2) is more than 5000-times smaller than the 30 μg/pulse reported by Reinhardt *et al.*[12] using their high laser energies (370 mJ, unknown fluence), which naturally results in our detection limits being 1–2 orders of magnitude higher than those of Reinhardt *et al.*[12]

The effective volume of our two-volume cryo-LA-cell of ~1–2 cm^3[13] contrasts the ~660 cm^3 of the cell used previously for IR-LA.[12] Consequently, our resultant rapid washout (~1.5 s for 99% signal decrease) facilitates depth-profiling (or continuous profiling) as a mode of analysis, which single volume LA cells with their inevitably large volume to accommodate ice slabs do not allow without significant mixing of signals. This is due to protracted signal washout related to the mean residence times as given by volume/flow rate.

Grain boundaries of ice crystals do not appear to represent an obstacle when ablating ice, because well developed ablation craters are formed straddling grain boundaries (Fig. 2). Using small circular (<100 μm) or especially rotatable rectangular spot sizes, this will in future be utilized to investigate whether noticeable cation concentration differences occur in the vicinity of grain boundaries in ice cores. It will allow us to investigate whether annual layer signatures from dust/sea salt are modified during ice formation/*in situ* recrystallization.

Acknowledgements

Equipment co-funding by a HEFCE SRIF3 and a RSF grant at RHUL is acknowledged. Comments by two reviewers helped to improve the manuscript.

Notes and references

1 W. Dansgaard, *Geochim. Cosmochim. Acta*, 1954, **6**, 241–260.

2 EPICA community members, *Nature*, 2006, **444**, 195–198.
3 North Greenland Ice Core Project members, *Nature*, 2004, **431**, 147–151.
4 EPICA community members, *Nature*, 2004, **429**, 623–628.
5 S. O. Rasmussen, K. K. Andersen, A. M. Svensson, J. P. Steffensen, B. M. Vinther, H. B. Clausen, M. L. Siggaard-Andersen, S. J. Johnsen, L. B. Larsen, D. Dahl-Jensen, M. Bigler, R. Rothlisberger, H. Fischer, K. Goto-Azuma, M. E. Hansson and U. Ruth, *J. Geophys. Res.–Atmospheres*, 2006, 111.
6 K. K. Andersen, A. Svensson, S. J. Johnsen, S. O. Rasmussen, M. Bigler, R. Rothlisberger, U. Ruth, M. L. Siggaard-Andersen, J. P. Steffensen, D. Dahl-Jensen, B. M. Vinther and H. B. Clausen, *Quat. Sci. Rev.*, 2006, **25**, 3246–3257.
7 J. P. Steffensen, K. K. Andersen, M. Bigler, H. B. Clausen, D. Dahl-Jensen, H. Fischer, K. Goto-Azuma, M. Hansson, S. J. Johnsen, J. Jouzel, V. Masson-Delmotte, T. Popp, S. O. Rasmussen, R. Rothlisberger, U. Ruth, B. Stauffer, M. L. Siggaard-Andersen, A. E. Sveinbjornsdottir, A. Svensson and J. W. C. White, *Science*, 2008, **321**, 680–684.
8 E. R. Thomas, E. W. Wolff, R. Mulvaney, S. J. Johnsen, J. P. Steffensen and C. Arrowsmith, *J. Geophys. Res.*, 2009, **114**, D08102.
9 J. Fluckiger, *Science*, 2008, **321**, 650–651.
10 S. G. Warren and R. E. Brandt, *J. Geophys. Res.*, 2008, **113**, D14220.
11 H. Reinhardt, M. Kriews, H. Miller, C. Ludke, E. Hoffmann and J. Skole, *Anal. Bioanal. Chem.*, 2003, **375**, 1265–1275.
12 H. Reinhardt, M. Kriews, H. Miller, O. Schrems, C. Ludke, E. Hoffmann and J. Skole, *Fresenius J. Anal. Chem.*, 2001, **370**, 629–636.
13 W. Müller, M. Shelley, P. Miller and S. Broude, *J. Anal. At. Spectrom.*, 2009, **24**, 209–214.
14 M. Guillong and C. A. Heinrich, *J. Anal. At. Spectrom.*, 2007, **22**, 1488–1494.
15 R. Garcia Fernandez, J. I. Garcia Alonso and A. Sanz-Medel, *J. Anal. At. Spectrom.*, 2004, **19**, 649–651.
16 D. Wilhelms-Dick, Ph.D. Thesis, Universität Bremen, 2008.
17 G. J. Weltje and R. Tjallingii, *Earth Planet. Sci. Lett.*, 2008, **274**, 423–438.